ISSN 1330-3651 (Print), ISSN 1848-6339 (Online)
Received: 25 June 2025; Accepted: 26 December 2025

https://doi.org/10.17559/TV-20250625002773
Original scientific paper

A Novel Wave-Induced Pneumatic Turbine Generator: Design, Performance Analysis, and Experimental Validation

Ali Ekber ÖZDEMİR

Abstract: This study proposes a wave-induced pneumatic energy converter that transforms vertical wave motion into airflow to produce electrical power. A laboratory-scale prototype was fabricated and tested by means of a Scotch-yoke mechanism that replicates wave-induced displacement. Owing to its compact architecture and reduced component count, the device can be manufactured at relatively low cost. Under regular-wave conditions (height = 0.5 m; period = 1 s), the mean outlet air velocity reached 30.72 ms^{-1} and the peak pneumatic power was 43.34 W. The measured energy-conversion efficiency was 25.71%, corresponding to a volumetric energy density of approximately 875 Wm^{-3}. Although the experiments were restricted to laboratory scale, the results confirm proof-of-concept. The observed performance and characteristics indicate potential for deployment in near-shore and off-shore environments; nevertheless, validation for full-scale sea conditions remains outside the scope of the present work.

Keywords: buoy system; experimental validation; pneumatic turbine; renewable energy; wave energy harvester

1 INTRODUCTION

Electrical energy is considered to be one of the most essential forms of energy for modern society, with an increasing demand on an annual basis [1]. However, this growing demand has resulted in higher CO2 emissions due to the continued dependence on fossil fuels for electricity generation [2]. Despite the notable advances in renewable energy sources, such as wind and solar power, their intermittent nature and geographical limitations necessitate the exploration of alternative, complementary energy solutions [3].

Among the various renewable energy sources, wave energy offers a vast, yet largely untapped potential. The global theoretical wave energy potential along coastlines has been estimated at approximately 2-3 TW [4]. Despite this potential, the contribution of wave energy to the total renewable energy generation remains minimal when compared to hydropower, wind, and solar systems [5-10]. The primary obstacles hindering the commercialisation of wave energy technologies pertain to corrosion, mechanical fatigue, and maintenance challenges arising from inclement marine conditions [11].

The concept of utilising ocean waves for energy purposes is not a recent innovation. The earliest known developments in this field date back to the 18th and 19th centuries [12-14], with significant progress occurring during the oil crisis of the 1970s, when research interest was renewed [15]. In recent years, a considerable number of prototypes have been developed; nevertheless, the majority of systems remain at the experimental stage due to their structural complexity and high production costs. Research is ongoing to achieve durable, efficient, and cost-effective designs capable of operating in real sea environments.

This study describes a wave-induced pneumatic energy conversion mechanism designed to transform vertical wave motion into pressurized airflow, which subsequently drives a turbine to generate electrical power. Unlike conventional oscillating water column systems, the proposed design isolates the mechanical components from seawater, thereby enhancing durability and reducing maintenance requirements. The design is characterised by its structural simplicity, reduced maintenance requirements and adaptability for small-scale applications. A laboratory-scale prototype was constructed and subjected to experimental testing to evaluate its pneumatic and electrical performance under controlled conditions.

The following section provides an overview of the primary forms of wave energy harvesting technologies, including the context for the proposed system.

2 AN OVERVIEW OF THE WAVE ENERGY HARVESTING TECHNOLOGY

Wave energy harvesting systems can be classified as shown in Fig. 1 [17].

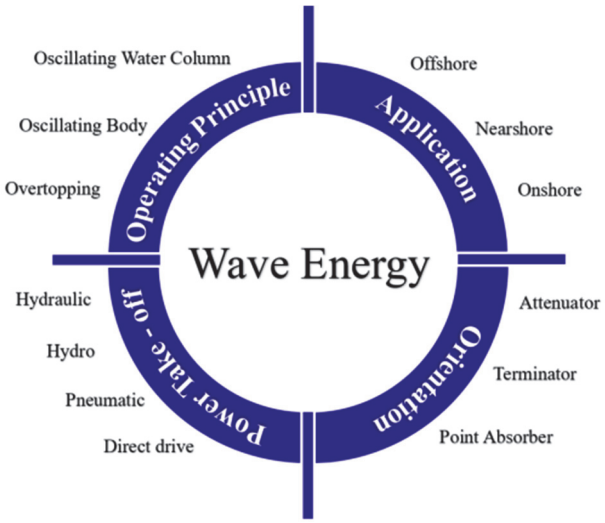

Figure 1 Wave energy classification

Energy can be extracted from waves through pneumatic, hydraulic, and mechanical methods. These energy extraction techniques, known as "Take-Off", systems, involve multiple stages of conversion to reach an output suitable for the electrical grid or supply to a load [17]. Mechanical energy can be extracted in a variety of ways and likewise can be converted into electrical energy using several methods including electromagnetic induction, piezoelectric, and triboelectric. [18]. The most

efficient system includes an induction-based electric generator driven by a mechanical mechanism. Electromagnetic induction-based generators (EMGs) fall under two groups, linear and rotary. A subset of these generators is given in Tab. 1 [17].

Table 1 List of generators used in a wave energy converter system

Rotational Generator	Linear Generator
Doubly Fed Induction	Longitudinal Flux Permanent Magnet
Squirrel Cage Induction	Variable Reluctance Permanent Magnet
Permanent Magnet Synchronous	Tubular Air-cored Permanent Magnet
Field Wound Synchronous	

EMGs have been widely used in large applications due to their higher energy conversion efficiency when the operating frequency is not low [19]. Tab. 2 compares the energy production capacity of wave energy harvesters using the different energy conversion methods [20-34].

Table 2 Energy production capacity of wave energy harvesters using different energy conversion methods

Method	Reference	Power output
Triboelectric Energy Conversion	[20]	15.2 Wm^{-3}
	[21]	13.23 Wm^{-3}
	[22]	2.04 Wm^{-3}
	[23]	5.38 Wm^{-3}
	[24]	23.2 Wm^{-3}
Piezoelectric Energy Conversion	[25]	5.73 Wm^{-3}
	[26]	206 Wm^{-3}
	[27]	≈ 12.66 Wm^{-3}
	[28]	18.8 Wm^{-3}
	[29]	70 Wm^{-3}
EMG	[30]	553 Wm^{-3}
	[31]	150.174 Wm^{-3}
	[32]	285.71 Wm^{-3}
	[33]	210 Wm^{-3}
	[34]	145.08 Wm^{-3}

For large-scale energy generation, not only should the output power of a wave energy device be considered, but also whether the material and construction methods are suitable for the proposed mechanism and appropriate for the environment.

Piezoelectric and Triboelectric energy conversion methods have advantages and disadvantages. A triboelectric nano-generator (TENG) based system can efficiently harvest energy at low frequencies [35] and is generally characterized by low weight and mass, as well as low fabrication cost [36]. However, TENGs have relatively low efficiency compared to other energy harvesting technologies, which can make them unsuitable for large-scale power generation. TENG devices generate electricity through friction, which will cause wear overtime, limiting the life of the devices and lead to the need for periodic maintenance or replacement. The performance of TENG devices can be affected by humidity, with high humidity reducing the efficiency of the devices and causing malfunction [37]. Piezoelectric energy conversion is an alternative energy conversion method. Although there has been research on wave energy harvesters based on piezoelectric energy conversion, it would not be suitable for large-scale applications due to its low power density.

EMG based systems are more suitable for large-scale applications. Hodgins et al. designed and built a 50 kW wave energy generator based on a permanent magnet linear generator [38], which would be suitable for use in large-scale power generation. Liu et al. designed and built a prototype of a permanent magnet linear generator with a maximum output power of 800 W [39]. Crowley et al [40] designed a floating body containing a pendulum system which has a maximum power generation capacity of 188 kW with an average capture factor of 0.59.

Small-scale laboratory systems are also common in literature. Miago et al. designed and tested a small wave energy harvester based on a rotating permanent magnet [41], which is particularly suitable for very low operating frequencies. Na et al [42] presented a wave energy harvester based on triboelectric energy conversion with 246 μW and 112.5 μW at matched loads of 40 MΩ and 200 MΩ, respectively. Such approaches can be used to supply power to low-power systems rather than large-scale applications.

Many technological approaches have been used for the mechanical conversion system. This includes oscillating water column (OWC), floating platforms and oscillating body systems. However, most of these systems have complex mechanical components that require high maintenance and incur high operating costs due to the harsh conditions in the marine environment. Most of the existing technologies are not commercially widespread, and research continues toward developing cost-effective and reliable solutions. Innovative designs that are more efficient and cost-effective are needed.

The novel wave energy harvesting system presented in this study is distinguished by its simple design and resilient construction. In comparison to other wave energy converters, the system has the primary benefit that its moving components are isolated from seawater, safeguarding against corrosion and mechanical wear. The system has been tested to determine efficiency under specific wave conditions, with promising results. Current development of wave energy technology has focused on highly efficient but complex mechanisms. However, simple and low-maintenance systems can offer significant advantages, particularly in areas with limited access to electricity, such as remote islands, coastal settlements, and offshore platforms. The results from this study confirm the feasibility of the proposed system at laboratory scale.

Recently, significant progress has been achieved in oscillating water column (OWC) systems, which represent one of the most mature and widely studied wave energy conversion technologies.

OWC devices operate by trapping air above an oscillating water surface, where the rise and fall of waves periodically compress and decompress the enclosed air, driving a bidirectional turbine to generate electricity.

Numerous large-scale OWC installations, such as the Mutriku plant in Spain and the Vizhinjam plant in India, have demonstrated the long-term operational feasibility of this principle.

Inspired by the same pneumatic energy conversion mechanism, the present study proposes a simplified and compact laboratory-scale prototype that replicates the indirect water contact of the OWC concept and offers a low-cost experimental framework for early-stage wave energy research.

The remaining sections of this study provide a detailed analysis of the structural features of wave energy

harvesting systems with a description of the design and construction of the proposed system.

3 DESIGN AND CONSTRUCTION OF THE HARVESTER

The laboratory-scale system proposed in this study functions as a wave-induced pneumatic turbine generator. The design consists of four primary components:

1- A vertical cylindrical chamber with a funnel-shaped bottom section and a flexible elastic diaphragm sealing the top,
2- A spherical mass placed directly on top of the elastic membrane,
3- A wind turbine positioned beneath the air outlet,
4- A guiding upper cylinder that restricts lateral displacement of the sphere during oscillation.

A schematic of the cross-sectional view and physical dimensions is shown in Fig. 2. The working principle relies on wave-induced vertical movement of the spherical mass. This motion deforms the elastic diaphragm, compressing the air inside the chamber. As the diaphragm is pushed downward, air is expelled through a narrow outlet, directed at the turbine blades. The resulting airflow induces rotational motion, allowing mechanical energy to be converted into electricity via an alternator.

The system operates in an analogous way to a pneumatic actuator, where the vertical motion of the mass compresses and expands the internal air volume. The elastic diaphragm acts as the transmission interface between the external wave excitation and internal air compression.

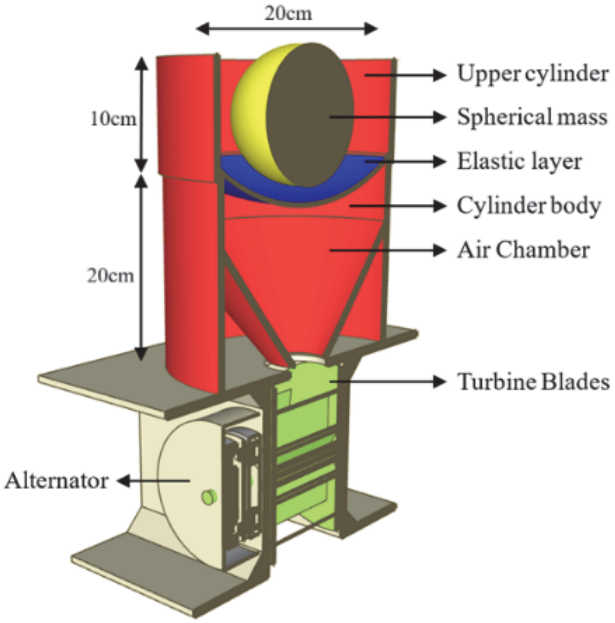

Figure 2 Cross-sectional view of presented wave energy harvester

To simulate variable loading conditions, the spherical mass was fabricated as a hollow 3D-printed shell with a wall thickness of 3 mm. This configuration allows easy adjustment of internal weight during experiments. The laboratory prototype is shown in Fig. 3, where the transparent casing and modular components enable visual monitoring and reconfiguration during test phases.

The overarching structure of the building is predicated on three key principles: compactness, simplicity, and adaptability.

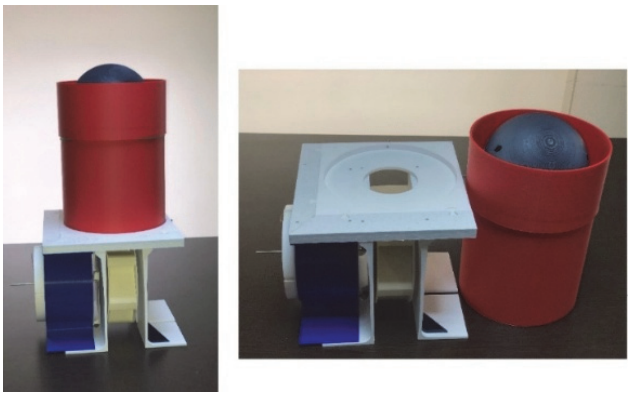

Figure 3 Laboratory-scale wave energy harvester

3.1 Theoretical Analysis of the Output Power of Wave Energy Harvesters

The proposed system operates by converting wave-induced vertical displacement into airflow, which in turn drives a turbine to generate electricity. In this section, a theoretical estimation of the maximum output power is presented based on fundamental thermodynamic and fluid dynamic principles.

When the spherical mass placed on top of the diaphragm moves downward due to wave action, it compresses the air within the lower chamber. This action generates airflow through the turbine located at the bottom outlet of the chamber. The expelled air volume can be approximated by the volume of a spherical cap, as shown in Fig. 4, and is calculated using Eq. (1) [43].

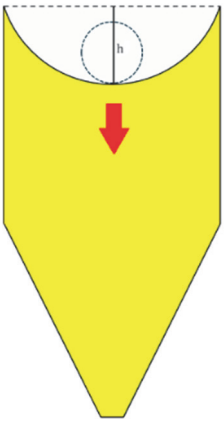

Figure 4 Air forced downwards by the movement of the mass above the system

$$\Delta V_{\text{air}} = \frac{\pi h^2 \left(3R - h\right)}{3} \tag{1}$$

where: ΔV is the volume of the spherical cap / m³, h is the height of the cap / m, R is the radius of the spherical mass / m ($R \leq 0.1$m).

The mechanical work done to compress the air under atmospheric pressure P_0 can be expressed by Eq. (2) [44]:

$$W_{\text{air}} = P_0 \Delta V \tag{2}$$

where: P_0 is atmospheric pressure (101325Pa), ΔV is the displaced air volume / m³.

Assuming the downward motion occurs in time t, the power output (idealized) is given by Eq. (3):

$$P_{\text{air}} = P_0 \frac{\pi h^2 (3R - h)}{3t} \tag{3}$$

For instance, a vertical displacement of 0.03 m occurring in 2 seconds yields an estimated output power of approximately 12.89 W under ideal conditions. Considering the total internal volume of the device is approximately 0.014725 m³, the volumetric energy density under ideal operation is:

$$\frac{12.89\ \text{W}}{0.014727\ \text{m}^{-3}} = 875.38\ \text{W m}^{-3}$$

However, real-world conditions introduce energy losses due to air leakage, friction, diaphragm hysteresis, and non-ideal compression. Considering typical energy conversion efficiencies for similar oscillating-body wave energy systems (30-50%) [45], the realistic energy density is expected to fall within the range of 262 to 437 Wm^{-3}.

These values serve as a baseline for evaluating experimental outcomes and are essential for benchmarking against other wave energy conversion technologies.

3.2 Numerical Simulation of Airflow Dynamics

A time-dependent numerical model was developed in COMSOL Multiphysics (v6.2, trial version) to complement the experimental analysis and to characterize the transient airflow behaviour inside the cylindrical chamber, converging funnel, and nozzle. The diaphragm motion was prescribed through a radially varying velocity profile expressed as:

$$V_{\text{dia}}(r,t) = A\left(1 - \left(\frac{r}{R_s}\right)^2\right)\sin\left(\frac{\pi t}{T_p}\right) \tag{4}$$

where: A is maximum displacement amplitude of the diaphragm / m, R_s is effective radius of the diaphragm surface / m, T_p is oscillation period corresponding to one full diaphragm cycle / s, r is radial coordinate measured from the symmetry axis / m, t is time variable / s.

A two-dimensional axisymmetric domain was constructed using the exact geometric dimensions of the prototype. Air properties were assigned from COMSOL's material library, and the unsteady laminar flow model was employed. A pressure-outlet boundary condition (0 Pa gauge) was imposed at the nozzle exit. Local mesh refinement was introduced around the funnel contraction and outlet to resolve steep velocity gradients. The simulation was executed over a full actuation period, and the surface-averaged outlet velocity magnitude was extracted as the primary performance indicator. The numerical model used the same operating parameters as the analytical formulation in Section 3.1, ensuring consistency between theoretical and computational evaluations.

The resulting velocity waveform at the nozzle exit is presented in Fig. 5. For a wave-induced actuation period of T = 2 s, the maximum predicted outlet velocity was approximately 3.36 m/s, whereas the corresponding laboratory measurement reached 9.25 m/s.

The discrepancy arises from physical effects not captured in the numerical model, namely:

(i) experimental mass induces a slightly larger diaphragm deflection than the prescribed amplitude, and

(ii) rotation of the turbine blades generates an additional suction effect at the nozzle exit, increasing the measured velocity. These mechanisms are absent in the simplified numerical representation, explaining the observed deviation.

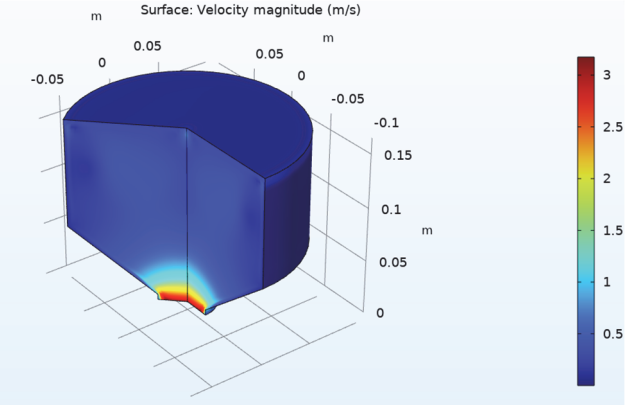

Figure 5 Surface-averaged outlet velocity magnitude at the nozzle exit obtained from the time-dependent numerical simulation

As demonstrated by Fig. 6, the flow accelerates transiently as it approaches the outlet region. The maximum velocity recorded was 3.36 m/s, which was observed in the proximity of the nozzle exit.

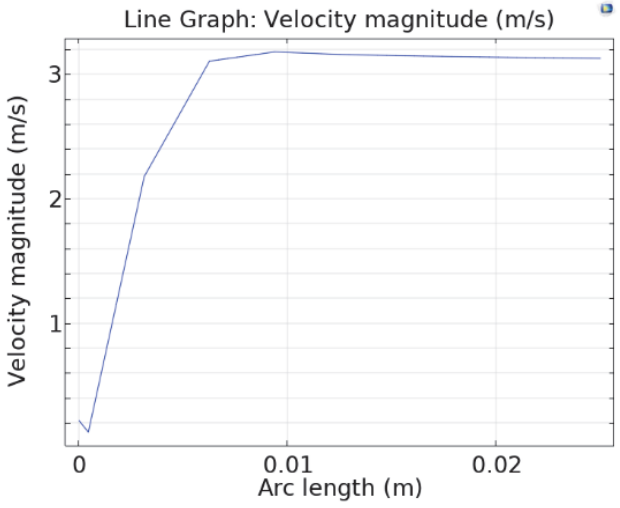

Figure 6 Velocity magnitude distribution along the nozzle centerline

4 EXPERIMENTS AND FINDINGS

To evaluate the performance of the proposed wave energy harvesting system, a laboratory-scale experimental setup was constructed as shown in Fig. 7.

The vertical motion of ocean waves was emulated using a Scotch yoke mechanism driven by a stepper motor. This configuration converts rotary motion into smooth, continuous reciprocating motion, which simulates the

vertical displacement induced by wave action. The motor speed was controlled by a MakerbaseMKSOSC driver board equipped with a manual potentiometer.

The outlet air velocity was measured using a UNI-T UT363S digital vane anemometer, which operates by correlating the rotational speed of a lightweight impeller with the local airflow velocity.

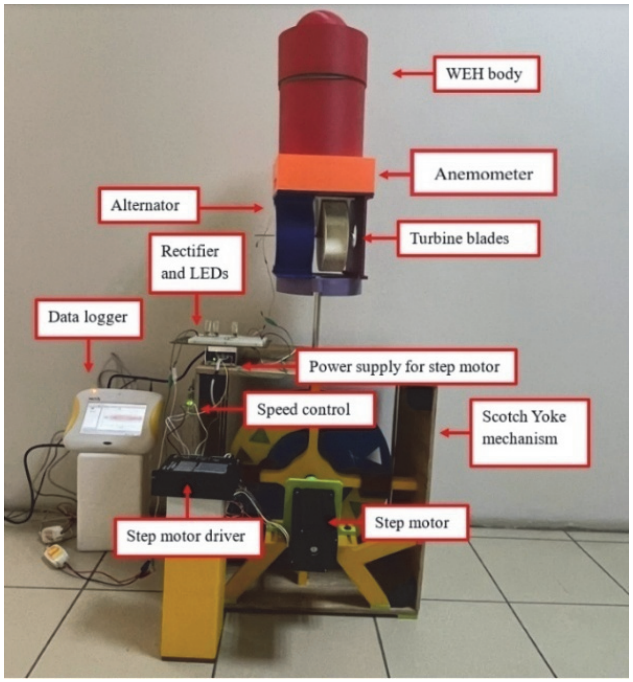

Figure 7 Experimental setup

The measurement range of the device is 0-30 ms^{-1}, with a resolution of 0.01 ms^{-1} and a manufacturer-specified accuracy of ±(5% + 0.5 ms^{-1}).

During testing, the anemometer was mounted inside the orange enclosure located directly above the alternator, as shown in Fig. 7. This location corresponds to the centerline of the outlet flow, approximately 2 cm downstream from the nozzle exit, ensuring that the sensor recorded the axial component of the high-speed airflow with minimal interference from boundary-layer and turbulence effects.

Each velocity measurement was repeated three times to ensure repeatability, and the average value was used for power and efficiency calculations. Considering both the instrument precision and calibration deviation, the combined measurement uncertainty was determined as ±3%, in agreement with the values reported in Tab. 3. This accuracy level is sufficient for characterizing the high-speed airflow (≈ 30 ms^{-1}) generated by the pneumatic compression mechanism.

Wave characteristics for the experimental conditions were based on real wave data from the Black Sea region. According to Akpınar and Kömürcü [46], significant wave periods along the southeastern coast of the Black Sea, including Ordu province, fall within the 0-3 s range, with wave heights between 0 m and 1.5 m being the most frequent. Based on these findings, the experimental wave parameters were chosen as 0.5 m height and 1 s and 2 s periods. The spherical mass was varied to determine its effect on system efficiency, with 2.5 kg found to be optimal.

4.1 Measurement Methodology

The electrical output of the single-phase permanent magnet alternator was rectified and measured through the setup shown in Fig. 8.

The alternator output was connected to a full-wave bridge rectifier consisting of four SS34 Schottky diodes (I_F = 3 A, V_{RRM} = 40 V). The rectifier output supplied a parallel combination of a filter capacitor (C_{out}) and a load resistor (R_{load}).

The output capacitor (C_{out} = 6800 µF / 25 V, low ESR) was used to smooth the voltage fluctuations at the rectifier output and to provide a stable DC voltage across the load. The optimum load resistance for maximum power transfer was determined by measuring the open-circuit voltage (V_{oc}) and short-circuit current (I_{sc}) of the alternator for a 1 s oscillation period using Eq. (5).

$$R_{load} = \frac{V_{OC}}{I_{SC}} \tag{5}$$

which yielded a value of approximately 16 Ω.

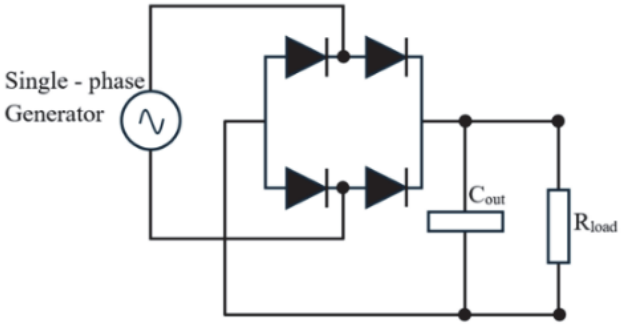

Figure 8 Electrical measurement system used in the experiment

The average airflow velocity directed at the turbine blades was measured for different wave periods. For the case of a 1-second wave period and 0.5 m wave height, the mean outlet velocity was measured as 30.72 m/s, as illustrated in Fig. 9.

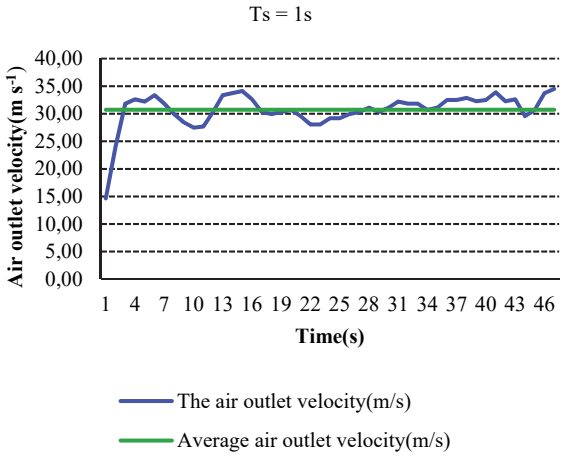

Figure 9 Air outlet velocity for wave period 1 s and wave height 0.5 m

Variations in airflow were primarily caused by the dual function of the outlet as both inlet and exhaust, combined with lateral movement of the spherical mass on the elastic

surface. The air velocity curve, along with the corresponding output voltage of the alternator, is shown in Fig. 10.

The voltage profile reflects the capacitor charging behaviour in the rectifier circuit. Output power was calculated using the kinetic energy by Eq. (6) [47]:

$$P = \frac{1}{2}\rho A V^3 \tag{6}$$

where: P is the pneumatic power /W, ρ = 1.225 kgm^{-3}, A = 0.00196 m^2 is the outlet cross-sectional area, V is the air velocity / ms^{-1}.

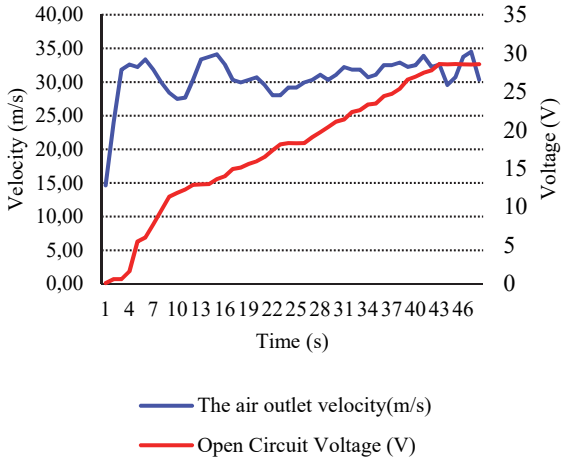

Figure 10 Air outlet velocity and open circuit voltage for wave period of 1 s

The maximum observed velocity was 33.03 ms^{-1}, corresponding to a peak power of 43.34 W, as shown in Fig.11.

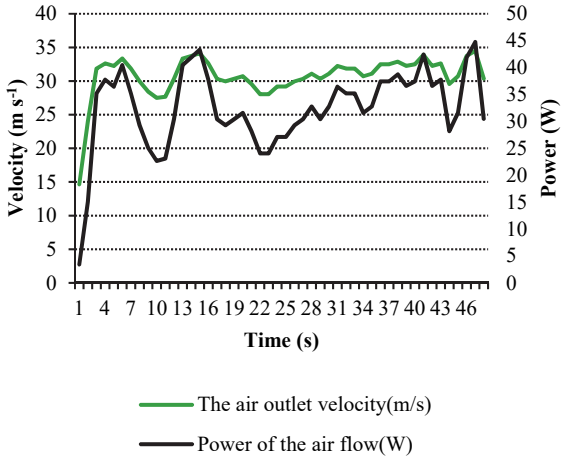

Figure 11 Air outlet velocity and air flow power for wave period of 1 s

The Mach and Reynolds numbers were estimated for the measured maximum air velocity to evaluate the flow regime. The Mach number was determined using Eq. (7)

$$M_a = V / a \tag{7}$$

where V = 30 m/s and a = 343 ms^{-1} is the speed of sound in air at 25 °C. This yields M_a = 0.087, indicating that the airflow is incompressible (M_a < 0.3). The Reynolds number was calculated from Eq. (8)

$$R_e = \frac{\rho V D}{\mu} \tag{8}$$

where: ρ is the air density, V is the mean outlet velocity (30 ms^{-1}), D is the nozzle diameter (0.05 m), and μ is the dynamic viscosity of air (1.8 × 10^{-5} Pas).

Substituting these values yields $R_e \approx 1.0 \times 10^5$, which corresponds to a fully turbulent flow regime at the nozzle exit.

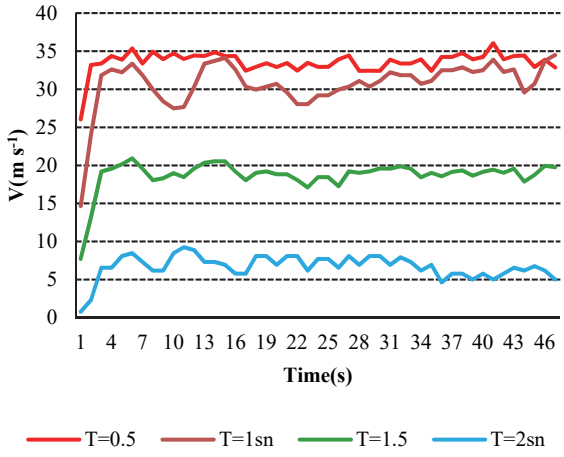

Figure 12 Effect of wave period on air outlet velocity

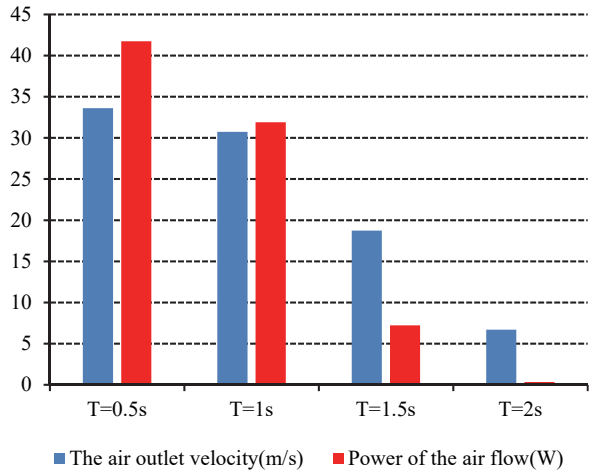

Figure 13 Average power and velocity of airflows corresponding to wave period

Airflow velocity and power were also evaluated as a function of wave period (Fig. 12 and Fig. 13). As expected, longer wave periods led to a reduction in outlet velocity and hence in power generation. For a wave period of 2.5 s, the airflow velocity was insufficient to generate meaningful electrical output.

This outcome is primarily due to the reduced acceleration of the spherical mass during longer periods, which limits air compression. Additionally, compressible flow dynamics impose a constraint known as the choking effect, where increasing pressure differential does not necessarily lead to higher flow velocity beyond a certain

threshold. The power of a wave can be calculated by the equation given in Eq. (9) from [48].

$$P_W = \frac{\rho_w g^2}{64\pi} H_s^{\,2} T \tag{9}$$

where: P_w is the power of the wave / Wm^{-1}, ρ_w is the density of water (approximately 1025 kgm^{-3} for seawater), g is gravitational acceleration (9.81 ms^{-2}), H_s is the significant wave height (typically twice the wave height), T is the wave period (s).

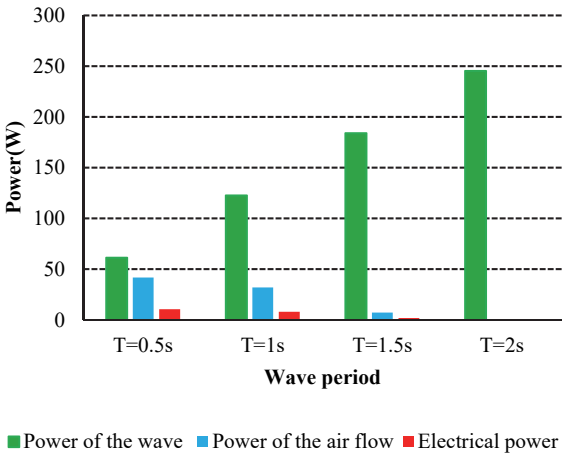

Figure 14 Variation of Wave Power, Airflow Velocity, and Electrical Power with Wave Period

Fig. 14 shows the output power of the proposed WEH is found to vary inversely proportional to the wave period. This phenomenon can be attributed primarily to the resonant frequency of the WEH. The underlying behaviour may be influenced by geometric scaling effects, which require further investigation before any conclusion on scale dependence can be drawn. However, this hypothesis will be investigated in future studies.

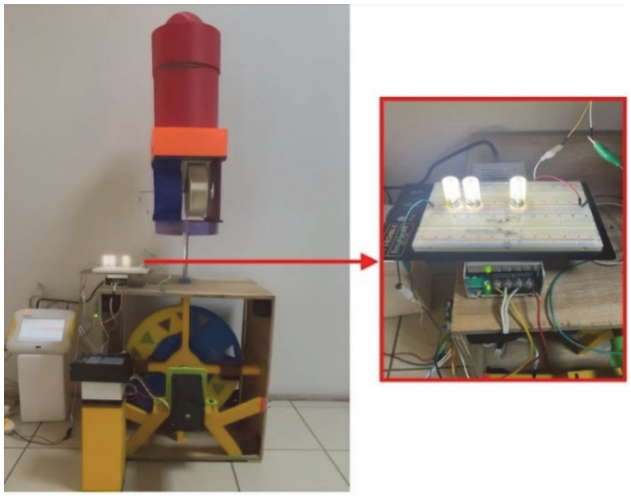

Figure 15 Illumination of 3 LEDs with a total power of 9 W with the electrical energy generated for 1 s wave period

The alternator used in the prototype was a custom-built 3D-printed generator incorporating permanent magnets. Due to design limitations, its conversion efficiency was limited to 25.71%, significantly lower than commercial alternators which typically range from 85% to 95%. This was identified as a major source of power loss.

Despite these limitations, the prototype successfully powered three 3 W LEDs under 1-second wave period conditions, as shown in Fig. 15. This proves the feasibility of using the system for practical low power applications and demonstrates the concept at laboratory scale. Performance can be enhanced with optimized turbine and generator designs.

4.2 Uncertainty Analysis

To quantify the reliability and precision of the experimental results, a comprehensive uncertainty analysis was conducted. The uncertainties associated with the primary measured and derived parameters are presented in this section. The overall uncertainty was evaluated based on the root-sum-square (RSS) method, considering both systematic (bias) and random (precision) errors [49].

Table 3 Summary of Key Uncertainties

Parameter	Value	Standard Uncertainty	Relative Uncertainty
Air Velocity / V	30.72 ms^{-1}	±0.93 ms^{-1}	±3.0%
Nozzle Diameter / d	0.05 m	±0.0005 m	±1.0%
Pneumatic Power / P	43.34 W	±3.94 W	±9.1%
System Efficiency / η	25.71%	±2.57%	±10.0%

The analysis confirms that the experimental findings are within acceptable uncertainty margins for a laboratory-scale prototype. The primary sources of uncertainty are the air velocity measurement and the efficiency of the custom-built electrical generator. Future work will employ higher-precision flow sensors and commercial-grade generators to reduce these uncertainties.

5 CONCLUSIONS

This study presented the design, construction, and experimental validation of a laboratory-scale wave-driven pneumatic turbine generator. The proposed system utilizes wave-induced vertical motion to compress air through an elastic diaphragm, which subsequently drives a turbine to generate electricity. One of the key advantages of the design is its structural simplicity and potential for long-term deployment in marine environments, where maintenance access is limited

Experimental results demonstrated that, under simulated wave conditions (0.5 m height and 1 s period), the system achieved a peak pneumatic power output of 43.34 W and an average airflow velocity of 30.72 ms^{-1}. Despite using a low-efficiency 3D-printed alternator, the system successfully powered a 9 W LED array, confirming the feasibility of the concept. The calculated energy conversion efficiency was 25.71% and the volumetric energy density reached approximately 875 Wm^{-3} under ideal conditions.

While promising, the prototype revealed two key limitations:

- The elastic diaphragm exhibited degradation over repeated cycles, leading to reduced responsiveness.
- The shared inlet-outlet design restricted continuous airflow, introducing fluctuations in power output.

To address these issues, future studies will assess candidate materials for the diaphragm (e.g., elastomer composites) under controlled fatigue and durability tests; this lies beyond the scope of the present work.

6 FUTURE WORK

Future efforts will focus on adapting the system design for potential application in real-world coastal and offshore environments. In the envisioned full-scale version, all moving parts will be fully isolated from seawater through a closed-loop pneumatic circuit, enhancing durability and minimizing corrosion-related failures.

A diaphragm-separated dual-chamber design will be used to generate internal pressure differentials, enabling sustained airflow within a sealed enclosure. Future work may explore CFD-based airflow simulations to gain further insight into optimization of the nozzle and turbine; however, this analysis lies beyond the scope of the present laboratory-scale study. Additionally, the use of commercial-grade alternators could be investigated to improve electrical conversion efficiency, particularly in larger or long-term deployments. Candidate diaphragm materials, such as elastomer composites, may also be evaluated in future durability and fatigue tests to enhance long-term performance.

Since the current system is a laboratory-scale prototype fabricated using 3D-printed components, techno-economic indicators such as levelized cost of energy (LCOE), durability, and long-term maintenance characteristics cannot yet be reliably assessed. These evaluations will be conducted in future work once a field-deployable full-scale prototype is constructed and operated under real wave conditions.

7 REFERENCES

[1] Abu Al-Haija, Q. (2021). A stochastic estimation framework for yearly evolution of worldwide electricity consumption. *Forecasting*, *3*(2), 256-266. https://doi.org/10.3390/forecast3020016

[2] Hasanuzzaman, M., Zubir, U. S., Ilham, N. I., & Seng Che, H. (2017). Global electricity demand, generation, grid system, and renewable energy policies: A review. *WIREs Energy and Environment*, *6*, e222. https://doi.org/10.1002/wene.222

[3] Energy: Global rise in electricity demand met entirely with renewables, report finds. (2022). *Engineering & Technology*, *17*(10), 5. https://doi.org/10.1049/et.2022.1008

[4] Wang, Z. L., Jiang, T., & Xu, L. (2017). Toward the blue energy dream by triboelectric nanogenerator networks. *Nano Energy*, *39*, 9-23. https://doi.org/10.1016/j.nanoen.2017.06.035

[5] Hassan, Q., Algburi, S., Sameen, A. Z., Al-Musawi, T. J., Al-Jiboory, A. K., Salman, H. M., Ali, B. M., & Jaszczur, M. (2024). A comprehensive review of international renewable energy growth. *Energy and Built Environment*. https://doi.org/10.1016/j.enbenv.2023.12.002

[6] Xia, H., Wang, X., Shi, J., Jia, N., & Duan, Y. (2022). Research on analysis method of tidal current energy resource characteristics. *Marine Technology Society Journal*, *56*(6), 10-17. https://doi.org/10.4031/MTSJ.56.6.5

[7] Procter, A. (2022). *Demand led tidal lagoon power and hydrogen energy storage: Supervisory control and optimisation*. University of South Wales.

[8] Tullos, D. (2009). Assessing the influence of environmental impact assessments on science and policy: An analysis of the Three Gorges Project. *Journal of Environmental Management*, *90*(Suppl. 3), S208-S223. https://doi.org/10.1016/j.jenvman.2008.07.031

[9] Stock, R. & Sovacool, B. K. (2023). Left in the dark: Colonial racial capitalism and solar energy transitions in India. *Energy Research & Social Science*, *105*, 103285. https://doi.org/10.1016/j.erss.2023.103285

[10] Wang, N., Kang, C., & Ren, D. (2016). Appendix A - China's 10 GW wind power base planning. *Large-scale wind power grid integration*, 313. https://doi.org/10.1016/B978-0-12-849895-8.15001-8

[11] Deligianni, A. & Drikos, L. (2023). Floating wave energy harvester: A new perspective. *Frontiers in Energy Research*, *11,* 1122154. https://doi.org/10.3389/fenrg.2023.1122154

[12] Clément, A., McCullen, P., Falcão, A., Fiorentino, A., Gardner, F., Hammarlund, K., Lemonis, G., Lewis, T., Nielsen, K., Petroncini, S., Pontes, M.-T., Schild, P., Sjöström, B.-O., Sørensen, H. C., & Thorpe, T. (2002). Wave energy in Europe: Current status and perspectives. *Renewable and Sustainable Energy Reviews*, *6*(5), 405-431. https://doi.org/10.1016/S1364-0321(02)00009-6

[13] Guo, B. & Ringwood, J. V. (2021). A review of wave energy technology from a research and commercial perspective. *IET Renewable Power Generation*, *15*, 3065-3090. https://doi.org/10.1049/rpg2.12302

[14] Falnes, J. (2007). A review of wave-energy extraction. *Marine Structures*, *20*(4), 185-201. https://doi.org/10.1016/j.marstruc.2007.09.001

[15] Aderinto, T. & Li, H. (2018). Ocean wave energy converters: Status and challenges. *Energies*, *11*(5), 1250. https://doi.org/10.3390/en11051250

[16] Babarit, A. (2017). Wave energy conversion historical perspective. *Wave energy conversion*, 37-98. https://doi.org/10.1016/B978-1-78548-264-9.50002-1

[17] Prasad, K. A., Chand, A. A., Kumar, N. M., Narayan, S., & Mamun, K. A. (2022). A critical review of power take-off wave energy technology leading to the conceptual design of a novel wave-plus-photon energy harvester for island/coastal communities' energy needs. *Sustainability*, *14*(4), 2354. https://doi.org/10.3390/su14042354

[18] Rahman, A., Farrok, O., Islam, M. R., & Xu, W. (2020). Recent progress in electrical generators for oceanic wave energy conversion. *IEEE Access*, *8*, 138595-138615. https://doi.org/10.1109/ACCESS.2020.3012662

[19] Barua, A. & Rasel, M. S. (2024). Advances and challenges in ocean wave energy harvesting. *Sustainable Energy Technologies and Assessments*, *61*, 103599. https://doi.org/10.1016/j.seta.2023.103599

[20] Liang, X., Liu, Z., Feng, Y., Han, J., Li, L., An, J., & Others. (2021). Spherical triboelectric nanogenerator based on spring-assisted swing structure for effective water wave energy harvesting. *Nano Energy*, *83*, 105836. https://doi.org/10.1016/j.nanoen.2021.105836

[21] Xu, L., Pang, Y., Zhang, C., Jiang, T., Chen, X., Luo, J., Tang, W., Cao, X., & Wang, Z. L. (2017). Integrated triboelectric nanogenerator array based on air-driven membrane structures for water wave energy harvesting. *Nano Energy*, *31*, 351-358. https://doi.org/10.1016/j.nanoen.2016.11.037

[22] Pan, L., Wang, J. et al. (2018). Liquid-FEP-based U-tube triboelectric nanogenerator for harvesting water-wave energy. *Nano Research*, *11*, 4062-4073. https://doi.org/10.1007/s12274-018-1989-9

[23] Liang, X., Liu, S., Lin, S., Yang, H., Jiang, T., & Wang, Z. L. (2023). Liquid-solid triboelectric nanogenerator arrays based on dynamic electric-double-layer for harvesting water wave energy. *Advanced Energy Materials*, *13*(24), 2300571. https://doi.org/10.1002/aenm.202300571

[24] Liu, S., Liang, X., Chen, P., Long, H., Jiang, T., & Wang, Z. L. (2023). Multilayered helical spherical triboelectric nanogenerator with charge shuttling for water wave energy harvesting. *Small Methods*, *7*(3), 2201392. https://doi.org/10.1002/smtd.202201392

[25] Peng, Y. et al. (2024). A self-powered and self-monitoring ultra-low frequency wave energy harvester for smart ocean ranches. *iScience*, *27*(9), 110665. https://doi.org/10.1016/j.isci.2024.110665

[26] Viet, N. V., Xie, X. D., Liew, K. M., Banthia, N., & Wang, Q. (2016). Energy harvesting from ocean waves by a floating energy harvester. *Energy*, *112*, 1219-1226. https://doi.org/10.1016/j.energy.2016.07.019

[27] Shan, X., Deng, J., Song, R., & Xie, T. (2017). A piezoelectric energy harvester with bending-torsion vibration in low-speed water. *Applied Sciences*, *7*(2), 116. https://doi.org/10.3390/app7020116

[28] Liu, H. X., Liu, M., Chai, Y. C. et al. (2019). Piezoelectric energy analysis on diverse buoy coupling with hydrodynamic parameters. *China Ocean Engineering*, *33*, 279-287. https://doi.org/10.1007/s13344-019-0027-3

[29] Pobering S. & Schwesinger N. (2004). A Novel Hydropower Harvesting Device. Proceedings of the 2004 International Conference on MEMS, NANO and Smart Systems (ICMENS'04), 480-485.

[30] Joe, H., Roh, H., Cho, H., & Yu, S.-C. (2017). Development of a flap-type mooring-less wave energy harvesting system for sensor buoy. *Energy*, *133*, 851-863. https://doi.org/10.1016/j.energy.2017.05.143

[31] Wang, C., Guo, L., Chen, P., Fu, Q., & Cui, L. (2023). Annular Electromagnetic Generator for Harvesting Ocean Wave Energy. *Journal of Marine Science and Engineering*, *11*(12), 2266. https://doi.org/10.3390/jmse11122266

[32] Li, Y., Chen, Z., Ma, X., Liu, H., Huang, M., Guo, Q., & Zhang, T. (2019). Design and experiment of an ultra-low frequency pendulum-based wave energy harvester. *2019 IEEE 14th International Conference on Nano/Micro Engineered and Molecular Systems (NEMS)*, 101-104. https://doi.org/10.1109/NEMS.2019.8915586

[33] Li, Y., Guo, Q., Huang, M., Ma, X., Chen, Z., Liu, H. et al. (2019). Study of an electromagnetic ocean wave energy harvester driven by an efficient swing body toward the self-powered ocean buoy application. *IEEE Access*, *7*, 129758-129769. https://doi.org/10.1109/ACCESS.2019.2937587

[34] Ren, H. & Wang, T. (2018). Development and modeling of an electromagnetic energy harvester from pressure fluctuations. *Mechatronics*, *49*, 36-45. https://doi.org/10.1016/j.mechatronics.2017.11.008

[35] Wu, S., Yang, J., Wang, Y., Liu, B., Xiong, Y., Jiao, H., Liu, Y., Bao, R., Wang, Z., & Sun, Q. (2023). UFO-shaped integrated triboelectric nanogenerator for water wave energy harvesting. *Advanced Sustainable Systems*, *7*(9), 2300135. https://doi.org/10.1002/adsu.202300135

[36] Barkas, D. A., Psomopoulos, C. S., Papageorgas, P., Kalkanis, K., Piromalis, D., & Mouratidis, A. (2019). Sustainable energy harvesting through triboelectric nanogenerators: A review of current status and applications. *Energy Procedia*, *157*, 999-1010. https://doi.org/10.1016/j.egypro.2018.11.267

[37] Wang, Z. L., Lin, L., Chen, J., Niu, S., & Zi, Y. (2016). *Triboelectric nanogenerators*. Springer. https://doi.org/10.1007/978-3-319-40039-6

[38] Hodgins, N., Keysan, O., McDonald, A. S., & Mueller, M. A. (2012). Design and testing of a linear generator for wave-energy applications. *IEEE Transactions on Industrial Electronics*, *59*(5), 2094-2103. https://doi.org/10.1109/TIE.2011.2141103

[39] Liu, C., Dong, R., & Ye, B.-L. (2022). Comprehensive sensitivity analysis and multi-objective optimization on a permanent magnet linear generator for wave energy conversion. *Renewable Energy*, *198*, 841-850. https://doi.org/10.1016/j.renene.2022.08.102

[40] Crowley, S., Porter, R., Taunton, D. J., & Wilson, P. A. (2018). Modelling of the WITT wave energy converter. *Renewable Energy*, *115*, 159-174. https://doi.org/10.1016/j.renene.2017.08.004

[41] Miao, G., Fang, S., Wang, S., & Zhou, S. (2022). A low-frequency rotational electromagnetic energy harvester using a magnetic plucking mechanism. *Applied Energy*, *305*, 117838. https://doi.org/10.1016/j.apenergy.2021.117838

[42] Jin, N., Mei, N., Zhang, D., & Zhong, Y. (2023). Triboelectric nanogenerators for efficient low-frequency ocean wave energy harvesting with swinging boat configuration. *Micromachines*, *14*(4), 748. https://doi.org/10.3390/mi14040748

[43] Shimabukuro, Y. E. (2022). Volume of intersection of a cone with a sphere. *arXiv*.

[44] Van Ness, H. C., Abbott, M., Swihart, M., & Smith, J. (2017). *Introduction to chemical engineering thermodynamics (8th ed.)*. McGraw-Hill Education.

[45] Aderinto, T. & Li, H. (2019). Review on power performance and efficiency of wave energy converters. *Energies*, *12*(22), 4329. https://doi.org/10.3390/en12224329

[46] Akpınar, A. & Kömürcü, M. İ. (2012). Wave energy potential along the south-east coasts of the Black Sea. *Energy*, *42*(1), 289-302. https://doi.org/10.1016/j.energy.2012.03.057

[47] Kalmikov, A. (2017). Chapter 2 - Wind power fundamentals. *Wind energy engineering*, 17-24. https://doi.org/10.1016/B978-0-12-809451-8.00002-3

[48] Liakatas, A., Galanis, G., Kalogeri, C., & Kallos, G. (2017). Wave power estimation by means of spectral wave models and satellite records. *Journal of Operational Oceanography*, *10*(1), 93-113. https://doi.org/10.1080/1755876X.2017.1289011

[49] Joint Committee for Guides in Metrology (JCGM). (2008). *Evaluation of measurement data - Guide to the expression of uncertainty in measurement*. International Organization for Standardization (ISO).

Contact information:

Ali Ekber ÖZDEMİR
Fatsa Faculty of Marine Sciences, Ordu University,
52400, Ordu, Turkey
E-mail: a.ekber@odu.edu.tr